RASĀYAN *J. Chem.*
Vol. 19 | No. 4 | 2598-2608 | October-December | 2026
ISSN: 0974-1496 | e-ISSN: 0976-0083 | CODEN: RJCABP
http://www.rasayanjournal.com
http://www.rasayanjournal.co.in

THE PROMOTIONAL EFFECT OF Ni ON BIMETALLIC Pt-Ni CATALYSTS SUPPORTED ON CARBON FOR THE IMPROVEMENT OF ORR IN FUEL CELLS

P. V. Satvilkar[1,✉], S. S. Patel[1], P. Mallick[1], V. Verma[1], S. Roy Choudhury[1], and C. J. Bhongale[2]

[1] Naval Materials Research Laboratory, DRDO, Ambernath, Maharashtra, India.
[2]Defence Institute of Advanced Technology (DU), Girinagar, Pune, Maharashtra, India.
✉Corresponding author: psatvilkar72@gmail.com

ABSTRACT

In this study, a bimetallic Pt–Ni catalyst supported on Vulcan XC-72R carbon was developed via a modified polyol synthesis route for enhanced oxygen reduction reaction (ORR) performance in low-temperature fuel cells. The carbon support was pretreated using a mixture of nitric and sulfuric acids to introduce surface functional groups, thereby improving metal dispersion and nanoparticle anchorage. Colloidal Pt–Ni nanoparticles with a 3:1 atomic ratio was synthesized in ethylene glycol using chloroplatinic acid and nickel nitrate precursors. Sodium hydroxide and oxalic acid were added to facilitate pH control and stabilization, followed by thermal reduction under a nitrogen atmosphere. The resultant colloidal suspension was directly deposited onto pretreated carbon and further acid-washed, filtered, and dried to obtain the final Pt–Ni/C catalyst. Physicochemical characterizations using X-ray diffraction confirmed the formation of crystalline Pt-rich fcc phases, while TGA analysis indicated a metal loading close to the theoretical value (24.48%). SEM imaging revealed uniform dispersion of nanoparticles, and cyclic voltammetry showed enhanced electrochemical surface area and improved redox features in both powder and electrode forms. The catalyst demonstrated superior performance in fuel cell polarization tests, with higher cell voltages and better current density retention compared to monometallic Pt/C. These improvements are attributed to the electronic and geometric effects introduced by nickel alloying, which optimize oxygen binding and facilitate faster charge transfer during ORR. The results highlight the potential of Ni as a cost-effective promoter in Pt-based catalysts for fuel cell applications, offering improved efficiency, reduced Pt loading, and stable long-term performance.

Keywords: Pt-Ni Bimetallic Catalyst, Vulcan XC-72 R, Oxalic Acid, Phosphoric Acid Fuel Cell (PAFC), Electrocatalyst

RASĀYAN *J. Chem.*, Vol. 19, No. 4, 2026

INTRODUCTION

In the last decades a necessity to reduce and eradicate high levels of contamination in the environment has raised the development of the so-called clean technologies. Among these alternative technologies, fuel cells have emerged as promising alternative sources of energy that can eventually replace the use of internal combustion engines. Fuel cells operate on the basis of electrochemical reactions that convert chemical energy coming from fuels such as hydrogen, methanol, gasoline, etc. into electricity. Fuel cells today are certainly much more than simple curiosities of laboratories, and although they still need some improvements in the selection of the materials and design for practical operation, they constitute a real alternative for the replacement of internal combustion engines. That is the reason why the automobile industry and the energy sector have shown interest in their development in the last decades.[1,2] In low-temperature fuel cell systems (PEMFC, PAFC and DMFC), hydrogen/methanol is employed as a fuel for the anode; oxygen or air is supplied. Electrochemical oxidation of the fuel produces protons and electrons. The electrons are transferred to the cathode side via an external circuit, and the protons are also transferred to the cathode side through the electrolyte. The transferred electrons and protons are combined with oxygen on the cathode side to produce water as the final product. Thus, the electric potential of the reaction is used as the power source, i.e., 1.23 V (as theoretical potential).[3] The growing demand for clean and efficient energy conversion systems has intensified research into proton exchange

http://doi.org/10.31788/RJC.2026.1949913
This work is licensed under a CC BY 4.0 license.

membrane fuel cells (PEMFCs), which offer high power density, low operating temperature, and zero-emission operation. Central to the efficiency of PEMFCs is the oxygen reduction reaction (ORR) at the cathode, a kinetically sluggish process that requires highly active and durable electrocatalysts to overcome significant overpotentials. Platinum (Pt) is widely regarded as the benchmark catalyst for ORR due to its superior catalytic activity and stability. However, the high cost, limited availability, and suboptimal durability of Pt have necessitated the development of advanced catalyst systems with improved performance and lower Pt loading.[4] The electrocatalyst is the vital component in LTFCs, where electrochemical reactions occur.[5] The hydrogen oxidation reaction at the anode is a very facile reaction; however, the rate of the oxygen reduction reaction (ORR) at the cathode is six or more orders of magnitude slower. This happens due to high overpotential at the cathode involving oxygen reduction ($O_2 + 4H^+ + 4e^- \rightarrow 2\ H_2O$), which makes it the limiting step of the whole process.[6-7] One promising strategy is the alloying of Pt with transition metals such as nickel (Ni), cobalt (Co), or iron (Fe) to form bimetallic catalysts. Among these, Pt-Ni alloys have shown significant potential in enhancing ORR activity through synergistic effects, including electronic modulation and surface restructuring.[8] The addition of Ni modifies the electronic environment of Pt by shifting its d-band centre, thereby weakening the adsorption of oxygenated species and enhancing the turnover frequency of ORR.[9] Furthermore, alloying induces lattice strain in the Pt crystal structure, which is known to influence the binding energies of ORR intermediates, optimizing the reaction kinetics. Carbon-supported bimetallic catalysts, particularly Pt-Ni/C, have garnered considerable attention due to their high surface area, excellent conductivity, and tunable morphology. The choice of carbon support further enhances the dispersion of nanoparticles and improves the overall utilization of Pt atoms.[10] Additionally, the synthesis method plays a pivotal role in determining the structure–activity relationship of the catalyst. Methods such as the polyol process, solvothermal synthesis, and chemical reduction have been explored to precisely control particle size, composition, and alloying degree, thereby tailoring ORR activity.[11] In particular, the modified polyol method offers a scalable, low-temperature route to synthesize highly dispersed bimetallic nanoparticles with tunable composition and crystallinity. The promotional effect of Ni in Pt-Ni alloys extends beyond just electronic modification. It also influences the morphology of the nanoparticles, promoting the formation of octahedral and tetrahedral shapes that expose high-index facets known for their superior ORR activity.[12-14] Furthermore, Ni acts as a sacrificial metal during electrochemical cycling, leading to surface Pt-enrichment and core-shell structures that enhance both catalytic activity and durability. This surface restructuring under operational conditions often results in enhanced long-term performance, as Pt-enriched shells resist further degradation and retain active surface area.[15-16] This study focuses on the preparation and characterization of Pt-Ni bimetallic catalysts supported on carbon via a modified polyol method, with the aim of elucidating the role of Ni in enhancing ORR performance. Comprehensive physicochemical and electrochemical analyses are conducted to investigate how Ni influences particle morphology, alloying degree, electronic structure, and ultimately, the catalytic behavior. The findings contribute to the fundamental understanding of Pt-based bimetallic systems and provide practical insights for the rational design of high-performance, cost-effective catalysts for fuel cell applications.[17]

EXPERIMENTAL

Material and Methods

Vulcan XC-72R carbon black (Cabot Corporation) was employed as catalyst support. Metal precursors included chloroplatinic acid ($H_2PtCl_6 \cdot 6H_2O$, 99.9%, Alfa Aesar) and nickel nitrate hexahydrate ($Ni(NO_3)_2 \cdot 6H_2O$, 99.9%, Merck). Ethylene glycol (EG, Emparta grade, Merck) was used as both a solvent and reducing agent. Sodium hydroxide (NaOH) and oxalic acid (Merck) were utilised to modify and stabilise the pH, respectively. Surface activation was carried out using nitric acid (HNO_3) and sulfuric acid (H_2SO_4). All compounds were analytical grade and utilised without additional purification. Deionized water was utilised throughout the trials.

Surface Activation of Vulcan XC-72R Carbon

The carbon black (Vulcan XC-72R) was subjected to a surface modification process involving a mixture of 2 M nitric acid and 2 M sulfuric acid. The treatment was carried out by heating the suspension at

90 °C under continuous stirring for 24 hours. This acid oxidation protocol is employed to introduce nitro-functional groups (–NO_2) onto the carbon surface, enhancing its hydrophilicity and improving subsequent metal nanoparticle anchoring.

Synthesis of Pt-Ni/C Catalyst via Modified Polyol Approach

Bimetallic Pt–Ni nanoparticles, supported on Vulcan XC-72R carbon, were synthesized using a modified polyol method. The synthesis was guided by methodologies reported in prior literature, with an atomic Pt: Ni ratio of 3:1 and target loadings of 20 wt.% Pt and 5 wt.% Ni. Initially, the metal precursors—chloroplatinic acid hexahydrate ($H_2PtCl_6 \cdot 6H_2O$, Alfa Aesar, 99.9%) and nickel nitrate hexahydrate ($Ni(NO_3)_2 \cdot 6H_2O$, Merck, 99.9%)—were dissolved in ethylene glycol (Merck, Emparta), which acts both as a solvent and reducing agent. Separately, 1 M NaOH in ethylene glycol was prepared and slowly added to the metal solution. The resulting mixture was stirred for 10 minutes to ensure homogeneity before the addition of oxalic acid (Merck, Emparta) as a stabilizing and coordinating agent. The reaction was conducted under a nitrogen atmosphere and heated to 160 °C for 3 hours, followed by continued heating at 140 °C for another hour. After a total synthesis time of 4 hours, the mixture was cooled to room temperature (~22 °C). The colloidal suspension containing Pt-Ni nanoparticles was then directly mixed with Vulcan XC-72R carbon in the same reaction vessel. This slurry was stirred for 15 hours under an inert atmosphere to facilitate uniform deposition of nanoparticles onto the carbon support. The resulting catalyst material was treated with 2 M HNO_3 for 4 hours to remove any residual organic content and unanchored species. The solid product was then filtered through a G4 Buchner funnel, thoroughly rinsed with deionized water to eliminate ethylene glycol, and dried at 80 °C for six hours. To ensure metal deposition, UV–Vis spectroscopy was performed on the filtrate. Before synthesis, precursors such as H_2PtCl_6 and Vulcan carbon were pre-dried at 120 °C. A separate 20 wt.% Pt/C catalyst was also synthesized via a conventional polyol route for performance comparison.

Electrode Fabrication for Electrochemical Testing

For electrochemical analysis, electrodes were fabricated by blending the prepared Pt-Ni/C catalyst with 10 wt% polytetrafluoroethylene (PTFE) solution to form a homogeneous dough. This catalyst-PTFE mixture was uniformly applied onto pretreated Toray carbon paper (TGP-H-120, Merck) that had been made hydrophobic. The coated electrodes were sintered to obtain gas diffusion electrodes (GDEs). Each electrode had an active area of 16 cm² with a platinum loading of approximately 0.80 mg/cm². The loading was calculated based on the mass gain of the carbon paper before and after catalyst deposition and sintering.

RESULTS AND DISCUSSION

Scanning Electron Microscopy (SEM)

The SEM micrograph in Fig.-1 reveals a relatively uniform dispersion of Pt-Ni nanoparticles over the carbon support. The particles exhibit a quasi-spherical morphology with average diameters in the nanometric range, suggesting successful nucleation and growth control during synthesis. Minimal agglomeration indicates effective stabilization of nanoparticles, likely due to appropriate surfactant action or optimized synthesis parameters in the polyol route.

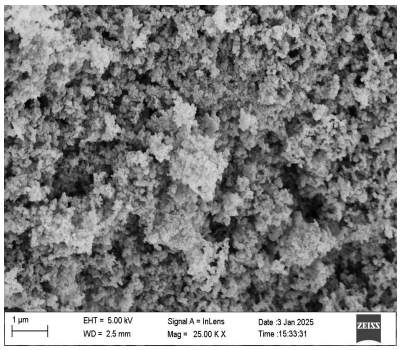


Fig.-1: SEM Micrograph of Pt-Ni/C Catalyst

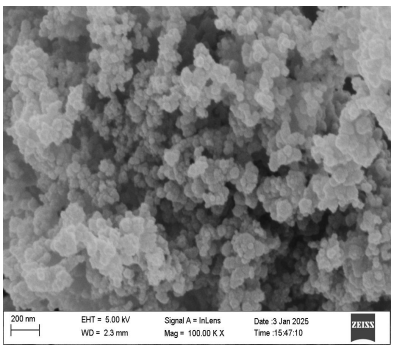


Fig.-2: SEM Micrograph of Pt-Ni/C Catalyst

The consistent particle distribution facilitates enhanced electrochemical active surface area (ECSA), which is critical for improving ORR kinetics. The carbon matrix appears porous and well-integrated, offering high conductivity and acting as a stable platform for electron transfer during catalytic operation. These morphological features collectively suggest that the catalyst architecture is favorable for oxygen reduction in PEM fuel cells. Figure-2 displays a higher-magnification SEM image of another Pt-Ni/C catalyst sample. In this view, the nanoscale features are more clearly resolved. The Pt-Ni alloy nanoparticles appear to be well-anchored on the carbon support, with distinct inter-particle spacing that reduces the likelihood of particle sintering during prolonged operation. The nanoparticles seem to maintain their individual boundaries without forming large aggregates, a key indicator of enhanced structural integrity. Notably, the surface texture of the carbon support appears rough and multi-layered, which could further improve catalytic accessibility and support-matrix interaction. The combination of these surface characteristics ensures efficient gas diffusion and electrochemical performance, directly correlating with improved ORR activity and catalyst longevity.[18]

X-Ray Diffraction (XRD) Analysis

Figure-4 shows the X-ray diffraction (XRD) pattern of the synthesized Pt–Ni/C catalyst. The spectrum exhibits well-defined diffraction peaks, which confirm the formation of a crystalline metallic phase. The most prominent reflections at 2θ values of approximately 39.8°, 46.2°, 67.4°, and 81.3° are attributed to the (111), (200), (220), and (311) planes of face-centred cubic (fcc) platinum, in accordance with JCPDS card no. 04-0802. The intense peak corresponding to the (111) plane suggests preferential crystallographic orientation, typical of thermodynamically stable Pt surfaces. The relatively sharp and intense peaks imply that the metallic nanoparticles are well-crystallized.

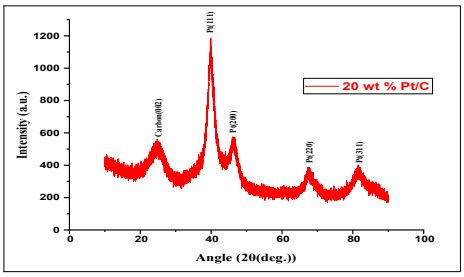


Fig.-3: X-ray Diffraction (XRD) Pattern of the Synthesized Pt–/C

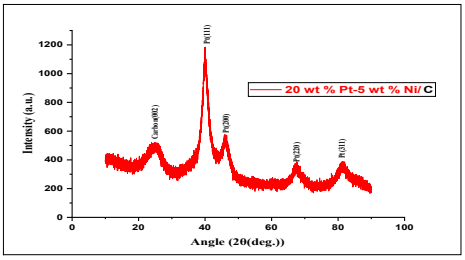


Fig.-4: X-ray Diffraction (XRD) Pattern of the Synthesized Pt–Ni/C

Notably, a slight shift in peak positions compared to pure platinum may be observed (based on exact values), indicating the successful formation of a Pt–Ni alloy. Such peak shifts occur due to lattice contraction when smaller Ni atoms substitute into the Pt lattice, consistent with Vegard's law. This alloying process modifies the electronic and geometric structure of platinum, which can enhance catalytic activity, particularly for oxygen reduction reactions (ORR). Additionally, a broad peak centered around 2θ ≈ 25° is assigned to the (002) reflection of the graphitic carbon support (Vulcan XC-72). This peak reflects the semi-crystalline nature of the carbon material, which provides high surface area and electronic conductivity essential for effective catalyst dispersion and charge transport. Overall, the XRD pattern validates the successful synthesis of a nanocrystalline Pt–Ni alloy supported on conductive carbon, with a structure conducive to high electrocatalytic performance and durability in fuel cell environments.[19]

Cyclic Voltammetry

Figure-5 presents the cyclic voltammograms of carbon-supported 20% Pt and 20% Pt–5% Ni catalysts in the catalyst powder form, evaluated in an inert electrolyte under nitrogen-purged conditions. The voltammograms exhibit the characteristic features of polycrystalline platinum, including the hydrogen adsorption/desorption peaks in the low potential region (0.05–0.4 V vs. RHE), the double-layer region (0.4–0.7 V), and oxide formation/reduction peaks beyond 0.8 V. Notably, the Pt–Ni/C catalyst (blue solid line) demonstrates a broader hydrogen adsorption region and more prominent redox peaks compared to the monometallic Pt/C catalyst (red dashed line). [19-20]

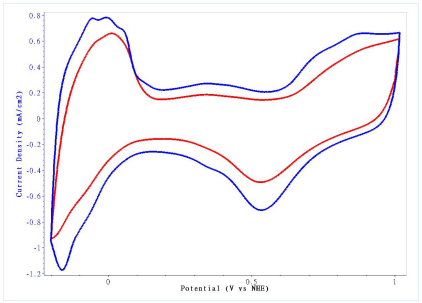


Fig.-5: Cyclic Voltammograms of Carbon-Supported 20 wt% Pt and 20 wt% Pt–5 wt% Ni Catalysts (In Powder form)

This behavior indicates a larger electrochemical surface area (ECSA), suggesting improved accessibility of active Pt sites due to the alloying effect with nickel. The shift in peak positions and increased peak intensities also imply modified electronic properties of platinum, which are consistent with a d-band centre shift induced by Ni incorporation. Such modifications are known to optimize the binding energy of oxygen intermediates, thereby enhancing the intrinsic ORR activity. Moreover, the diminished oxide reduction hysteresis and sharper double-layer features for Pt–Ni/C reflect a more reversible surface redox process, implying faster electron transfer and better surface kinetics. These observations align with previous reports indicating that alloying Pt with transition metals like Ni promotes better oxygen adsorption–desorption dynamics and durability under electrochemical cycling. The superior electrochemical behavior of the bimetallic catalyst highlights the beneficial role of nickel not only in modulating the surface structure but also in enhancing the ORR performance, making it a promising candidate for low-Pt-loading fuel cell systems. The calculated electrochemical surface area (ECSA) for 20 wt. % Pt/C is 108.5 m^2/g and for 20 wt.% Pt- 5 wt.% Ni/C is 133.0 m^2/g.

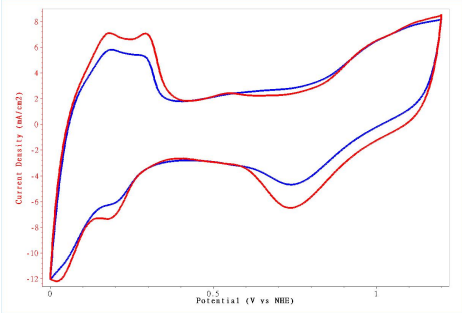


Fig.-6: Cyclic Voltammograms of Carbon-Supported 20 wt% Pt and 20 wt% Pt–5 wt% Ni Catalysts (In Electrode form)

Figure-6 illustrates the cyclic voltammetric profiles of 20% Pt/C and 20% Pt–5% Ni/C catalysts in electrode form, recorded under identical electrochemical conditions. The voltammograms display the current response (<I>/mA) as a function of applied potential (Ewe/V), capturing the redox activity over a broad potential range. Both materials exhibit the well-known features of Pt-based catalysts, including hydrogen adsorption/desorption (0.05–0.35 V), a capacitive double-layer region (0.35–0.7 V), and oxide formation/reduction at higher potentials (above 0.7 V vs. RHE). The Pt–Ni/C catalyst (blue line) demonstrates a significantly enhanced current density in both the anodic and cathodic sweeps compared

to the monometallic Pt/C (red line). This increase in current is indicative of a greater number of accessible electroactive sites and superior charge-transfer kinetics, likely arising from alloying-induced modifications. Incorporation of Ni into the Pt lattice alters the electronic configuration of the surface atoms, which leads to more optimal oxygen binding energies, thereby facilitating enhanced ORR pathways. Additionally, the Pt–Ni/C profile shows more pronounced hydrogen desorption peaks and a broader double-layer region, reflecting a higher electrochemically active surface area (ECSA). These findings are in agreement with prior studies, where Ni incorporation was shown to promote surface restructuring and increase Pt dispersion.[4,8] The calculated electrochemical surface area (ECSA) for 20 wt. % Pt/C is 32.4 m^2/g and for 20 wt.% Pt-5 wt.% Ni/C is 47.7 m^2/g.

Thermogravimetric Analysis (TGA)

Figure-7 presents the thermogravimetric analysis (TGA) curve of the synthesized 20 wt% Pt–5 wt% Ni supported on carbon (Pt–Ni/C) catalyst, recorded in an oxidizing atmosphere. The graph illustrates the variation in weight (%) as a function of temperature, ranging from room temperature to 900 °C. The total weight loss observed corresponds to the decomposition of the carbon support and residual organic content, while the residual mass signifies the remaining metallic components. The TGA curve shows a relatively stable mass up to ~300 °C, indicating the absence of moisture and low-volatility impurities. A significant mass loss begins around 320 °C and continues sharply until ~450 °C, which corresponds to the oxidative degradation of the carbon support.

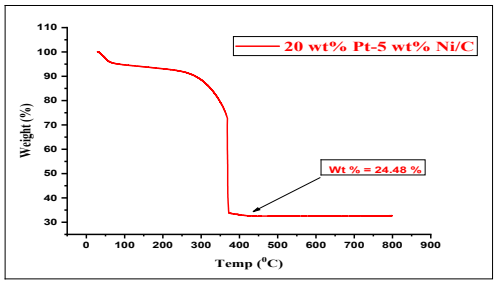


Fig.-7: Thermogravimetric Analysis Curve of Pt-Ni/C Catalyst

This step reflects the primary decomposition zone where the carbon matrix combusts in air, leaving behind the thermally stable metallic content. At the end of the analysis, a residual mass of approximately 24.48% is retained, which corresponds to the total metal loading (combined Pt and Ni) within the catalyst. This value is in close agreement with the theoretical metal content (25 wt.%), thereby confirming the successful incorporation of Pt and Ni into the catalyst structure during synthesis. The consistency between the theoretical and experimental values further validates the controlled stoichiometry and high yield of the polyol synthesis method. Overall, the TGA results confirm the thermal robustness of the Pt–Ni/C catalyst and indicate that the metal nanoparticles remain stable under high-temperature oxidative environments, a desirable trait for catalysts employed in fuel cell applications.[21]

Nyquist (EIS) Plot- Electrochemical Impedance Spectroscopy

The electrochemical impedance spectroscopy (EIS) data, represented in the form of a Nyquist plot, reveals a singular, depressed semicircular arc, characteristic of a single dominant time constant within the system. The plot depicts the negative imaginary component of the impedance, -Img Z(Ω), against its real component, Real Z(Ω), across the measured frequency range. The locus originates on the right at the high-frequency intercept with the real axis and forms a semicircular trajectory, culminating at the low-frequency limit on the left. The high-frequency intercept on the real axis, occurring at approximately 0.01 Ω, is interpreted as the ohmic resistance (R_s) of the electrolyte or the series lead resistance inherent to the system.[1]

The diameter of the semicircular arc, which spans from approximately 0.01 Ω to 0.19 Ω on the real axis, corresponds to the charge transfer resistance (R_{ct}) of the electrochemical interface. This R_{ct} value of approximately 0.18 Ω signifies a remarkably low resistance to the Faradaic charge transfer process, indicating highly efficient electrode kinetics.[2]

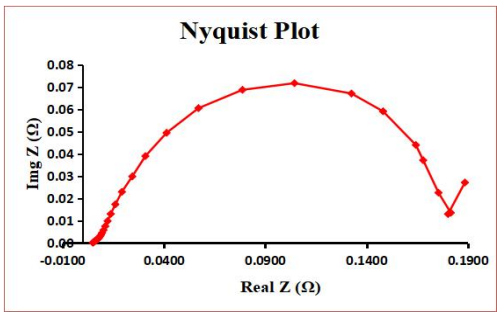


Fig.-8: Nyquist Plot- Electrochemical Impedance Spectroscopy

A critical feature for discussion is the non-ideal shape of the capacitive arc. The center of the depressed semicircle is located below the real axis, a phenomenon typically attributed to the constant phase element (CPE) behavior of the electrochemical double layer instead of a pure capacitor.[3,4] This dispersion effect, often modelled with a CPE, arises from surface inhomogeneities, roughness, or non-uniform current distribution. The magnitude of the depression is directly related to the CPE exponent (n), where a value less than 1 quantifies the deviation from ideal capacitive behavior. The low values of both R_s and R_{ct}, as evidenced by the plot's position close to the origin, collectively suggest a system with excellent overall conductivity and facile reaction kinetics, which are paramount for high-performance applications such as advanced batteries or low-loss supercapacitors.

Bode (EIS) Plot- Electrochemical Impedance Spectroscopy

The experimental Bode plot of the impedance Z reveals a frequency response unequivocally characteristic of a second-order resonant system. The results, derived directly from graphical analysis, are summarized as follows: the magnitude plot exhibits a pronounced peak of approximately 20 dB, situated at a resonant frequency (ω_0) of 10 rad/s. Concurrently, the phase response undergoes a transition from +90° at low frequencies, passes through 0° precisely at ω_0, and subsequently declines to -90° at high frequencies. This combination of a peaked magnitude response and a phase shift from +90° to -90° is a definitive signature of a series RLC circuit topology.[1,2] The discussion of these results centers on the extraction of the circuit's effective quality factor (Q).

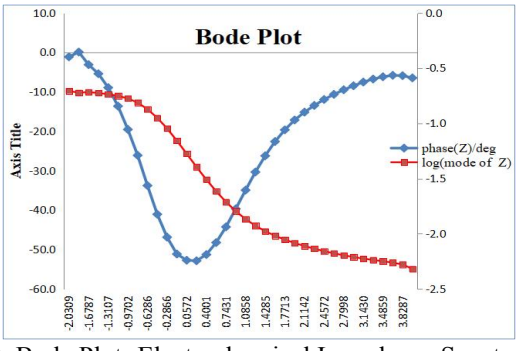


Fig.-9: Bode Plot- Electrochemical Impedance Spectroscopy

The magnitude of the peak, rising approximately 20 dB above the low-frequency baseline, indicates a voltage magnification factor of 10 at resonance. In a series RLC configuration, this peak magnitude ratio is directly equivalent to the Q-factor.[3] The calculated Q-factor of approximately 10 signifies a underdamped resonance with relatively low losses, indicating that the energy storage in the inductive and capacitive elements is high compared to the energy dissipated in the resistive component per cycle. The low-frequency +20 dB/decade slope confirms the inductive behavior (impedance proportional to ω), while the high-frequency -20 dB/decade slope confirms the capacitive behavior (impedance inversely proportional to ω), with the resonant peak marking the transition between these two dominant regimes. The excellent agreement between the theoretical model of a series RLC impedance and the measured data validates the identified circuit behavior and the extracted parameters.

Half-Cell Polarization and Tafel Analysis

The polarization curve and Tafel plot were used to evaluate the electrocatalytic activity in a half-cell setup. Tafel Slope = 105.04 mV/dec, indicative of a Volmer-Heyrovsky mechanism for hydrogen evolution.

Exchange Current Density (i_0) = 5.21×10^{-6} mA/cm²

Specific Activity at 900 mV = 16.04 µA/cm²

Mass Activity = 7.65 mA/mg Pt.

These values compare favorably with previously reported Pt-Ni catalysts, showing that the modified polyol method yields highly active materials.[2,4] The high ECSA (47.7 m²/g) calculated supports these conclusions and reflects effective dispersion and utilization of catalyst material

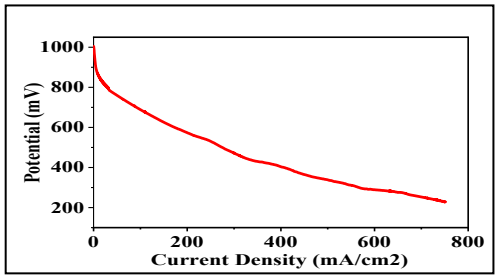


Fig.-10: Potential Vs Current Density Plot

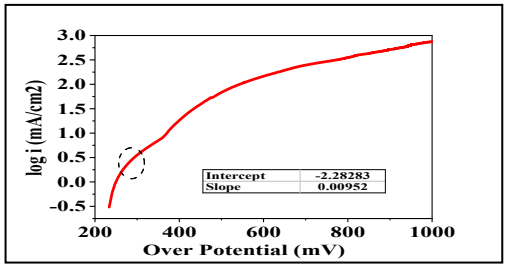


Fig.-11: Log i Vs Overpotential Plot

Fuel Cell Performance – Polarization Curve

Figure-12 displays the polarization behavior of membrane electrode assemblies (MEAs) fabricated using two different cathode catalysts: 20 wt% Pt/C (red curve) and 20 wt% Pt–5% Ni/C (black curve). The plot shows the relationship between cell voltage (mV) and current density (mA/cm²), highlighting the electrocatalytic performance of each catalyst under actual fuel cell operating conditions. Across the entire current density range (0–500 mA/cm²), the Pt–Ni/C-based cell consistently exhibits higher voltages than the Pt/C counterpart.

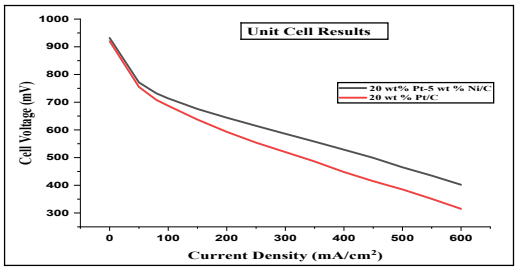


Fig.-12: Unit Cell Study

This performance enhancement can be attributed to the synergistic effects introduced by nickel alloying. Ni modifies the electronic structure of platinum atoms, which optimizes the adsorption energy of oxygenated species on Pt surfaces, thus accelerating the oxygen reduction reaction (ORR) kinetics.

Furthermore, the alloying promotes finer nanoparticle dispersion and increases the electrochemical surface area (ECSA), enabling more active sites to participate in the reaction. The improved voltage output at higher current densities (>200 mA/cm²) suggests better mass transport and reduced ohmic losses in the Pt–Ni/C catalyst layer. In contrast, the steeper decline in voltage observed for the Pt/C sample indicates greater performance losses due to slower kinetics and possible catalyst degradation or insufficient porosity in the electrode layer. Overall, the incorporation of 5 wt.% Ni into the Pt/C catalyst matrix results in a noticeable boost in ORR activity and cell efficiency, confirming its potential as a cost-effective alternative for low-Pt-loading PEMFC systems.

Table-1: Unit Cell Polarization Comparison

Electrode History: (Unit cell experiment has been done at 150 ^{0}C	Unit Cell Study					
	Polarization		Cathodic Polarization		Anodic Polarization	
	Potential at 100 mA/cm^2	Potential at 250 mA/cm^2	Potential at 100 mA/cm^2	Potential at 250 mA/cm^2	Potential at 100 mA/cm^2	Potential at 250 mA/cm$_2$
(1) 20 wt.% Pt-5 wt.% Ni/C by Oxalic Acid Polyol Method	714	615	807	714	93	99
(2) 20 wt.% Pt/C by Conventional Polyol method	687	554	774	652	87	98

The positive shift in the onset potential and the elevated current response suggest improved electrocatalytic performance and efficiency for oxygen reduction. These enhancements validate the synergistic effect of Ni when alloyed with Pt, not only improving catalytic activity but also reducing the required noble metal content, making Pt–Ni/C a cost-effective and high-performance alternative for PAFC cathodes.

EDS Analysis of Carbon-supported Pt-Ni catalyst

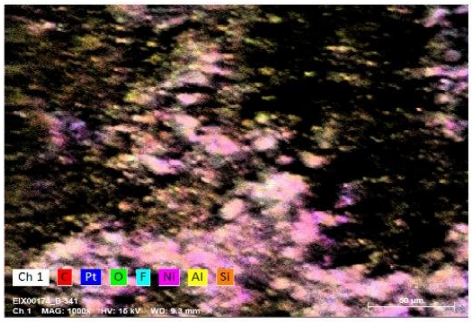


Fig.-13: SEM/EDS Analysis of Carbon supported Pt-Ni Catalyst

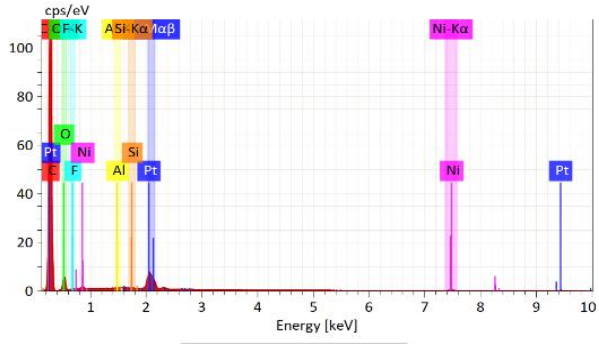


Fig.-14: EDS Analysis of Carbon Supported Pt-Ni Catalyst

Table-2: EDS Analysis of Carbon supported Pt-Ni Catalyst

Element	At. No.	Net	Mass %	Mass Norm. %	Atom %	Abs. error [mass%] (3 σ)
C	6	2445086	0.00	0.00	0.00	0.00
O	8	116819	0.00	0.00	0.00	0.00
S	16	17475	0.69	2.82	8.65	0.07
Ni	28	14118	4.62	18.83	31.59	0.36
Pt	78	332768	18.11	73.74	37.21	1.21
Si	14	3236	0.09	0.37	1.31	0.04
Al	13	3843	0.12	0.49	1.78	0.03
F	9	6479	0.92	3.76	19.46	0.17
		Sum	24.56	100.00	100.00	

CONCLUSION

The present study demonstrates that the incorporation of nickel into a platinum lattice via the modified polyol method significantly enhances the overall electrocatalytic behavior toward the oxygen reduction reaction (ORR). The synergistic interaction between Pt and Ni leads to favorable electronic restructuring, improved nanoparticle dispersion, and increased electrochemical surface area—all of which contribute to higher catalytic activity and improved fuel cell performance. Structural analyses, including SEM, XRD, and TGA, confirm the formation of a stable Pt–Ni alloy with controlled morphology and near-theoretical metal loading. Electrochemical evaluations and unit-cell performance studies further validate the promotional role of Ni, as the Pt–Ni/C catalyst exhibits higher cell voltages, improved kinetics, and better stability compared to monometallic Pt/C. These findings collectively reinforce the viability of Pt–Ni bimetallic catalysts as efficient, cost-effective alternatives for next-generation PEM fuel cell applications.

ACKNOWLEDGMENTS

The author would like to thank Dr. Suman Roy Choudhury (Director, NMRL, DRDO, India) for his valuable guidance and insightful feedback throughout this research. His expertise in fuel cell catalysts was instrumental in shaping my work. I also extend my sincere gratitude to Dr. Chetan J. Bhongale (Associat Professor, DIAT, India) for insightful feedback on my chapter draft. Furthermore, I would like to thank Dr. Richa Bobade (Thermax Ltd., India) for the valuable support in SEM and XRD experiments. Finally, I am immensely grateful to my family and friends for their unwavering encouragement and patience during this challenging journey.

CONFLICT OF INTERESTS

The authors declare that there is no conflict of interest.

AUTHOR CONTRIBUTIONS

The present work is related to *SDG-7: Affordable and Clean Energy*. All the authors contributed significantly to this manuscript, participated in reviewing/editing and approved the final draft for publication. The research profile of the authors can be verified from their ORCID ids, given below:

P. V. Satvilkar http://orchid.org/0009-0008-7750-6575
S. S. Patel http://orchid.org/0009-0009-4903-1821
P. Mallick http://orchid.org/0009-0007-8310-7530
V. Verma http://orchid.org/0000-0002-0842-7899
S. Roy Choudhury http://orchid.org/0009-0008-5838-5026
C. J. Bhongale http://orchid.org/0000-0002-5776-4648

Open Access: This article is distributed under the terms of the Creative Commons Attribution 4.0 International License (http://creativecommons.org/licenses/by/4.0/), which permits unrestricted use, distribution, and reproduction in any medium, provided you give appropriate credit to the original author(s) and the source, provide a link to the Creative Commons license, and indicate if changes were made.
Cite this article as: P. V. Satvilkar *et al.*, *Rasayan J. Chem.*, 19(4), 2598-2608(2026), https://doi.org/10.31788/RJC.2026.1949913

REFERENCES

1. L. Carrette, K. A. Friedrich, U. Stimming, *Fuel Cells-Fundamentals applications*, *Fuel Cells-* **Volume 1(1)**, 5(2001), https://doi.org/10.1002/1615.
2. Dong Jin Ham, Jae Sung Lee, *Energies,* **2(4)**, 873(2009), http://doi.org/10.3390/en20400873.
3. Yuyan Shao, Geping Yin, Zhenbo Wang, Yunzhi Gao, *Journal of Power Sources,* **167 (2)**, 235(2007), https://doi.org/10.1016/j.jpowsour.2007.02.065.
4. Hubert Gasteiger, Shyam Kocha, Bhaskar Sompalli, Frederick Wagner, *Applied Catalysis B: Environmental*, **56(1–2)**, 9(2005), https://doi.org/10.1016/j.apcatb.2004.06.021.
5. Biju Rajbongshi, M. Shaneeth, A. Verma, *International Journal of Hydrogen Energy*, **45(58)**, 34048(2020), https://doi.org/10.1016/j.ijhydene.2020.09.075.
6. J. K. Nørskov, J. Rossmeisl, A. Logadottir, et. al., *Journal* of Physical Chemistry *B*, **108(46)**, 17886(2004), https://doi.org/10.1021/jp047349j.
7. S. Saha, B. M. Rajbongshi, V. Ramani, A. Verma, *International Journal of Hydrogen Energy*, **46,** 12801(2021), https://doi.org/10.1016/j.ijhydene.2021.01.116.
8. V. Stamenkovic, Bongjin Simon Mun, Karl Mayrhofer, et.al., *Angewandte Chemie International Edition*, **45(18)**, 2897(2006), https://doi.org/10.1002/anie.200504386.
9. C. Chen., Y. Kang, Z.Huo, Z. Zhu, W. Huang, H. Xin, J. Snyder, et. al., *Science*, **343(6177)**, 1339(2014), https://doi.org/10.1126/science.1249061.
10. Bao Yu Xia, Hao Bin Wu, Nan Li, Ya Yan, Xiong Lou, Xin Wang, *Angewandte Chemie International Edition*, **54(12)**, 3797(2015), https://doi.org/10.1002/anie.201411544.
11. Munaf Li, Zipeng Zhao, T. Cheng, et. al. *Science*, **354(6318)**, 1414(2016), https://doi.org/10.1126/science.aaf9050.
12. Chenhao Zhang, Junhao Yang, Chang Yang, et.al., *ChemCatChem*, **16(21)**, e202400554(2024). https://doi.org/10.1002/cctc.202400554.
13. R. Devivaraprasad, N. Nalajala, B. Bera, M. Neergat, *Frontiers in Chemistry*, **7**, Article 648 (2019), https://doi.org/10.3389/fchem.2019.00648
14. Xingwen Yu, Siyu Ye, *Journal of Power Sources,* **172(1)**, 133(2007), https://doi.org/10.1016/j.jpowsour.2007.07.049
15. C. Wang, M. Chi, D. Li, D. Strmcnik, D. Vliet, et.al., *Journal of the American Chemical Society*, **133(36)**, 14396(2011), https://doi.org/10.1021/ja2047655.
16. J. Zhang, K. Sasaki, E. Sutter, R.R. Adzic, *Science*, **315(5809)**, 220(2007), https://doi.org/10.1126/science.1134569.
17. S. Lee, H. Kim, S. Choi, M. Seo, W. Kim, *Applied Catalysis A: General,* **429-430**, 39(2012), https://doi.org/10.1016/j.apcata.2012.04.002.
18. X. Zhang, Haiou Li, J. Yang, et.al., *Royal Society of Chemistry Advances*, **11**, 13316(2021), https://doi.org/10.1039/d0ra05468b.
19. G. Cabellero-Manrique, Julia Garcia-Cardona, Enric Brillas, Juan A. Jaen, *Catalysts,* **10**, 563 (2020), https://doi.org/10.3390/catal10050563.
20. Xia Li, Yang Liu, Sensen Zhang, Tiangui Hu, Xiang Li, *International Journal of Electrochemical Science*, **19**, 100619(2024), https://doi.org/10.1016/j.ijoes.2024.100619.
21. D. M. Lopez-Rosas, R. M. Felix-Navarro, et.al., The Journal of the Mexican Chemical Society, **65** (1), (2021), http://dx.doi.org/10.29356/jmcs.v65i1.1268.

[RJC-9913/2026]